RESEARCH ARTICLE

Journal of COMPUTATIONAL CHEMISTRY **WILEY**

Hydride and halide abstraction reactions behind the enhanced basicity of Be and Mg clusters with nitrogen bases

Manuel Yáñez[1] ⓘ | **Otilia Mó**[1] | **M. Merced Montero-Campillo**[1] |
Ibon Alkorta[2] ⓘ | **José Elguero**[2]

[1]Departamento de Química, Módulo 13, Facultad de Ciencias, and Institute for Advanced Research in Chemical Sciences (IAdChem), Universidad Autónoma de Madrid, Campus de Excelencia UAM-CSIC, Cantoblanco, Madrid, Spain

[2]Instituto de Química Médica, IQM-CSIC, Madrid, Spain

Correspondence
Manuel Yáñez, Departamento de Química, Módulo 13, Facultad de Ciencias, and Institute for Advanced Research in Chemical Sciences (IAdChem), Universidad Autónoma de Madrid, Campus de Excelencia UAM-CSIC, Cantoblanco, 28049 Madrid, Spain.
Email: manuel.yanez@uam.es

Ibon Alkorta, Instituto de Química Médica, IQM-CSIC, Juan de la Cierva, 3. 28006 Madrid, Spain.
Email: ibon@iqm.csic.es

Abstract

In this study, we investigate the protonation effects on the structure, relative stability and basicity of complexes formed by the interaction of monomers and dimers of BeX_2 and MgX_2 (X = H, F) with NH_3, CH_2NH, HCN, and NC_5H_5 bases. Calculations were performed using the M06-2X/aug-cc-pVTZ formalism, along with QTAIM, ELF and NCI methods for electron density analysis and MBIE and LMO-EDA energy decomposition analyses for interaction enthalpies. The protonation of the MH_2^- and M_2H_4–Base complexes occurs at the negatively charged hydrogen atoms of the MH_2 and M_2H_4 moieties through typical hydride abstraction reactions, while protonation at the N atom of the base is systematically less exothermic. The preference for the hydride transfer mechanism is directly associated with the significant exothermicity of H_2 formation through the interaction between H^- and H^+, and the high hydride donor ability of these complexes. The basicity of both, MH_2 and M_2H_4 compounds increases enormously upon association with the corresponding bases, with the increase exceeding 40 orders of magnitude in terms of ionization constants. Due to the smaller exothermicity of HF formation, the basicity of fluorides is lower than that of hydrides. In Be complexes, the protonation at the N atom of the base dominates over the fluoride abstraction mechanism. However, for the Mg complexes the fluoride abstraction mechanism is energetically the most favorable process, reflecting the greater facility of Mg complexes to lose F^-.

KEYWORDS
DFT calculations, fluoride abstraction, hydride abstraction, intrinsic basicity, Mg and Be clusters, nitrogen bases

1 | INTRODUCTION

A fundamental characteristic of electron-deficient systems is their behavior as strong Lewis acids. This ability to accept electron density transferred from a Lewis base inevitably enhances the intrinsic acidity of the base. This phenomenon is well-documented experimentally and theoretically, particularly for phosphineboranes, which exhibit an increase in acidity by 16–18 orders of magnitude compared to their corresponding phosphines, as measured by ionization constants.[1,2] Subsequent studies have shown that replacing boron with other elements in the same group results in similarly substantial acidity enhancements in complexes between triels and various electron-deficient compounds

with different bases,[3–9] including also some oxyacids.[10] In specific cases, these acidity enhancements can lead to spontaneous proton transfer[11] or loss of H_2.[12]

In a recent paper, we investigated the capacity of clusters of Be and Mg derivatives to substantially enhance the acidity of typical nitrogen bases.[13] Our findings indicate that this enhancement increases with the size of the cluster, from monomers to trimers. It is also evident that the intrinsic basicity of the Lewis acid is likely to be altered to some extent. This prompted us to investigate the protonation effects on the structure, relative stability, and basicity of the same set of complexes, formed when the monomers and dimers of BeX_2 and MgX_2 (X = H, F) interact with ammonia, methaneimine, hydrogen cyanide, and pyridine. Our study extended beyond monomers because our previous research showed[13] that the effects of these interactions on acidity vary with the size of the Be and Mg clusters involved. All monomers and dimers of MX_2 (M = Be, Mg; X = H, F) exist in the gas phase, but the information about their intrinsic thermodynamic properties is rather scarce. To date, their gas-phase basicity has never been reported, and the gas-phase acidity is known only for the two hydrides.[14] Mg_2F_4 is formed by equilibrium vaporization of MgF_2 in the temperature range 1200–1540 K,[15] whereas Be_2H_4 and Mg_2H_4 have been synthesized by the reaction of laser-ablated Be and Mg atoms, respectively, with molecular hydrogen.[16,17]

1.1 | Computational details

The protonation of the complexes MX_2–Base and M_2X_4–Base (M = Be, Mg; X = H, F; Base = ammonia, methaneimine, hydrogen cyanide, and pyridine) was analyzed using the M06-2X DFT approach associated with an aug-cc-pVTZ basis set. This theoretical model accounts for dispersion effects[18] and yields enthalpies and free energies in good agreement with the G4 theory,[19] particularly when dealing with electron-deficient compounds.[13,20,21]

The bonding characteristics of the neutral and protonated complexes were analyzed using the quantum theory of Atoms in Molecules (QTAIM) approach.[22] This method involves a topological analysis of the molecular electron density, $\rho(\mathbf{r})$, to locate and characterize its critical points, namely bond-, ring-, and cage-critical points. The electron density and its Laplacian at the bond critical points (BCPs) provide information about the strength and covalency of the chemical linkage and permit to define the molecular graph that provides important structural information. These calculations were performed using the AIMAll (Version 19.10.12) code.[23]

A complementary view of the electron density distribution within the complex can be obtained using the electron localization function (ELF) method.[24] This approach locates areas with a low value of the excess local kinetic energy associated with highly localized electrons, allowing the definition of monosynaptic basins (typically associated with core and electron lone pairs) and disynaptic (or polysynaptic) basins (associated with two-center or multi-center bonding interactions). Polysynaptic basins, particularly trisynaptic ones, are common

in electron-deficient compounds, which are prone to form three-center two-electron (3c, 2e) bonds, such as those stabilizing diborane.

As we will discuss in the following sections, many of the complexes investigated are stabilized by weak intermolecular interactions, where the van der Waals component significantly contributes to the strength of these interactions. These weak interactions are often overlooked when using AIM or ELF formalisms but can be detected with the NCIPLOT approach,[25] which identifies regions of low reduced density gradients and low electron density values, which are typically associated with such interactions.

The analysis of the stability trends of the complexes investigated was facilitated by two different energy decomposition methods: the many-body interaction energy (MBIE) formalism,[26,27] and the localized molecular orbital energy decomposition analysis LMO-EDA.[28] The MBIE method decomposes the total binding energy of the molecular systems into one-, two-, three-center, or n-center ($n > 3$) terms as indicated in Equations (2)–(4), respectively, providing a detailed understanding of the interactions within the complexes.

$$\Delta E = E(ABC) - \sum_{i=A}^{C} E_m(i) = \sum_{i=A}^{C} E_R(i) + \sum_{i=A}^{B} \sum_{j>i}^{C} \Delta^2 E(i,j) + \Delta^3 E(ABC)$$

$$(1)$$

$$E_R(i) = E(i) - E_m(i) \tag{2}$$

$$\Delta^2 E(ij) = E(ij) - [E(i) - E(j)] \tag{3}$$

$$\Delta^3 E(ABC) = E(ABC) - [E(A) + E(B) + E(C)] - [\Delta^2 E(AB) + \Delta^2 E(AC) + \Delta^2 E(BC)] \tag{4}$$

The one-center terms, $E_R(i)$, represent the energetic cost of distorting each monomer within the cluster. This is calculated as the difference between $E_m(i)$, the energy of the i-monomer in its equilibrium geometry, and $E(i)$, the energy of the i-monomer within the geometry of the ABC complex. The two- and three-body interaction energies, $\Delta^2 E(ij)$ and $\Delta^3 E(ABC)$ computed at the corresponding geometries in the complex, quantify the stabilization (or destabilization) associated with these interactions in the ABC system.

In the LMO-EDA[28] procedure, the interaction energy is given by the equation:

$$E_{int} = E_{elec} + E_{exc} + E_{rep} + E_{pol} + E_{disp} \tag{5}$$

The first term, E_{elec}, describes the classical coulombic interaction between the occupied orbitals of the monomers. The second and third terms, E_{exc} and E_{rep}, represent the exchange and repulsive components associated with the Pauli exclusion principle. The fourth term, E_{pol}, accounts for polarization effects, and fifth term, E_{disp}, accounts for dispersion effects. Unlike the MBIE method, the LMO-EDA interaction energy, based on the generalized Kohn-Sham (GKS) approach, does not include the distortion energy. These LMO-EDA calculations were carried out using the GAMESS code (version 2012-R1).[29]

2 | RESULTS AND DISCUSSION

2.1 | MH₂-base complexes (M = Be, Mg)

We will start our discussion by analyzing the results obtained for the MH₂–Base complexes (M = Be, Mg: Base = NH₃, CH₂NH, HCN, C₅NH₅). According to the molecular electrostatic potential (MEP) of MH₂ compounds (see Figure 1), the π-hole is distributed as a belt around the H–M–H axis, while the areas favorable to electrophilic attacks are associated with the hydrogen atoms.

Consistently, the protonation of these compounds occurs at the negatively charged hydrogen atoms through a typical hydride abstraction reaction. Accordingly, the protonated species can be seen as the interaction between an MH⁺ closed-shell cation and a hydrogen molecule (see Figure 2).

Hydride abstraction reactions are not uncommon in chemistry, particularly in processes involving transition-metal cations and anions,

as well as neutral systems.[30–33] These hydride abstraction mechanisms play significant roles in organic synthesis,[34,35] in catalysis,[36–38] and in biochemical processes.[39] Many studies have attempted to quantify the hydride donor ability of various species.[40–42] Our work focuses on processes in the gas phase, whereas most previous studies mentioned above have been conducted in solution. In our case, the hydride abstraction follows a proton attack.

When analyzing the MH₂–NH₃ cluster, the most significant change in the MEP (see Figure 1) is the position of the π-holes, now associated with the hydrogens of NH₃. The electrophilic areas remain associated with the hydrogens of the BeH₂ moiety but are more attractive than in the isolated compound. Thus, a possible mechanism for the protonation of the MH₂–Base complex is again a hydride abstraction reaction, resulting in the formation of a H₂ molecule. Hence, the protonated species results from the interaction between a [MH–Base]⁺ closed-shell cation and H₂ (structure **A** in Figure 2). A second protonation process, which involves protonation at the N of

FIGURE 1 Molecular electrostatic potential for BeH₂ and its complex with NH₃. The black dots denote the existence of π-holes, which in BeH₂ form a belt around the H–Be–H axis and in the BeH₂–NH₃ complex are associated with the hydrogens of NH₃. Red areas are favorable for electrophilic attacks.
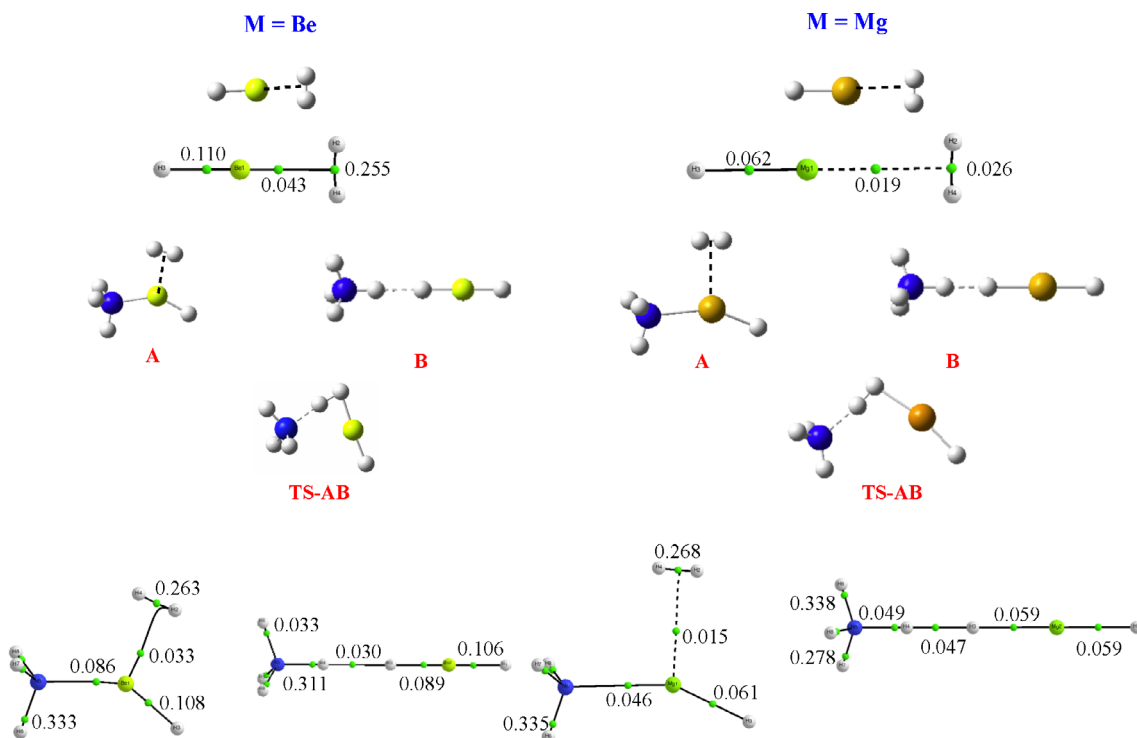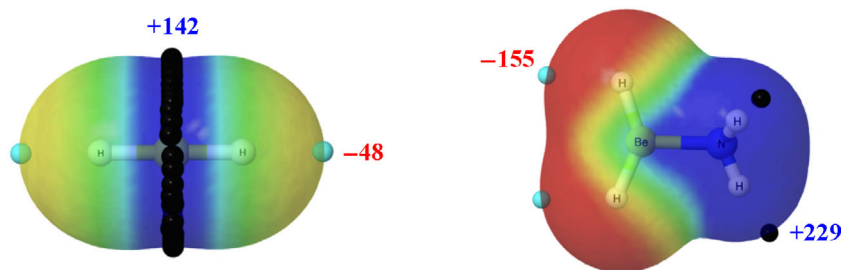

FIGURE 2 Structures and molecular graphs for protonated forms of BeH₂, MgH₂, and their complexes with NH₃. The structures of the transition states (**TS-AB**) connecting forms **A** and **B** are also provided. Electron densities at the BCPs are in a.u.

the base, is also possible. In this case, the final protonated form is a complex between MH_2 and the protonated base, $BaseH^+$, stabilized by the formation of a dihydrogen bond (DHB)[43-45] (structure **B** in Figure 2). Both protonated forms are illustrated in the second row of Figure 2, using the complex with ammonia as a suitable example. The structures for the other bases are shown in Figure S1.

The conversion from isomer **A** to isomer **B** through the transition state **TS-AB** (see Figure 2) involves high activation barriers, as shown in Table S1, which also includes the geometries of the transition states for the other bases. The proton affinities (PA) of the isolated MH_2 compounds and their complexes with NH_3, CH_2NH, HCN, and NC_5H_5, yielding structures **A** and **B** are given in Table 1.

The first outstanding finding is that, for both Be and Mg complexes, the protonation of the MH_2–Base at the metal yielding $[MH–Base]^+\cdots H_2$ is energetically more favorable than protonation at the N atom of the base, which yields $[MH_2–BaseH]^+$. This can be

understood through thermodynamic cycles that outline the different steps leading from the initial complex to the two different final products. These cycles, illustrated using the $BeH_2–NH_3$ complex as an example, are shown in Figure 3. In Figure S2, an alternative view of the energetics of both possible processes is provided.

For the process yielding $[BeH–Base]^+\cdots H_2$, the first step involves the loss of H^-, which is a rather endothermic process, resulting in a $[BeH–Base]^+$ closed-shell cation. This is followed by the protonation of H^- to form an H_2 molecule in a highly exothermic reaction. The final step is the interaction between H_2 and the $[BeH–Base]^+$ closed-shell cation, leading to the final product with slight exothermicity.

In the second process, in which the $[BeH_2–BaseH]^+$ species is the final product, the first step is the dissociation of the initial BeH_2–Base cluster, which is endothermic by 95 kJ·mol^{-1}. This is followed by the protonation of NH_3, defining the proton affinity of this base. Finally, the interaction between the BeH_2 and NH_4^+ yields the final product, $[BeH_2–NH_4]^+$.

An analysis of both thermodynamic cycles reveals that the mechanism leading to $[BeH–Base]^+\cdots H_2$ as the final product is the most exothermic due to the significant exothermicity of forming the H_2 molecule through the protonation of H^-. Thus, although the loss of H^- is quite endothermic (813 kJ·mol^{-1}), the overall process of forming $[MH–Base]^+ + H_2$ is more exothermic (−853 kJ·mol^{-1}) than the protonation of NH_3 (−837 kJ·mol^{-1}). This energetic difference becomes even more pronounced when considering that the dissociation of the initial complex is endothermic by 95 kJ·mol^{-1}.

The second important finding is the spectacular increase in the intrinsic basicity of the MH_2 hydride after its attachment to the different bases (see Table 1). For example, in the $BeH_2–NH_3$ complex shown in Figure 2, the basicity of the BeH_2 compound increases by 230 kJ·mol^{-1} upon attachment to NH_3, which translates to an increase of more than 40 orders of magnitude in terms of the

TABLE 1 Proton affinities (PA) and proton affinity enhancements (ΔPA) of MH_2 and MH_2–Base complexes. All values are in kJ·mol^{-1}.

M = Be				M = Mg		
Compound	A	B	ΔPA	A	B	ΔPA
MH_2	641.2	–	0.0	802.3		0.0
MH_2–NH_3	871.6	780.3	230.4	929.2	833.6	126.8
MH_2–$NHCH_2$	887.5	783.8	246.3	937.6	836.9	135.2
MH_2–NCH	868.1	704.9	226.9	939.1	–[a]	136.8
MH_2–NC_5H_5	914.9	825.9	273.7	957.4	874.8	155.0

Note: The PAs of NH_3, $NHCH_2$, HCN and NC_5H_5 are: 837, 855, 698 and 918 kJ·mol^{-1}, respectively. Values in bold refer to the most basic isomer.
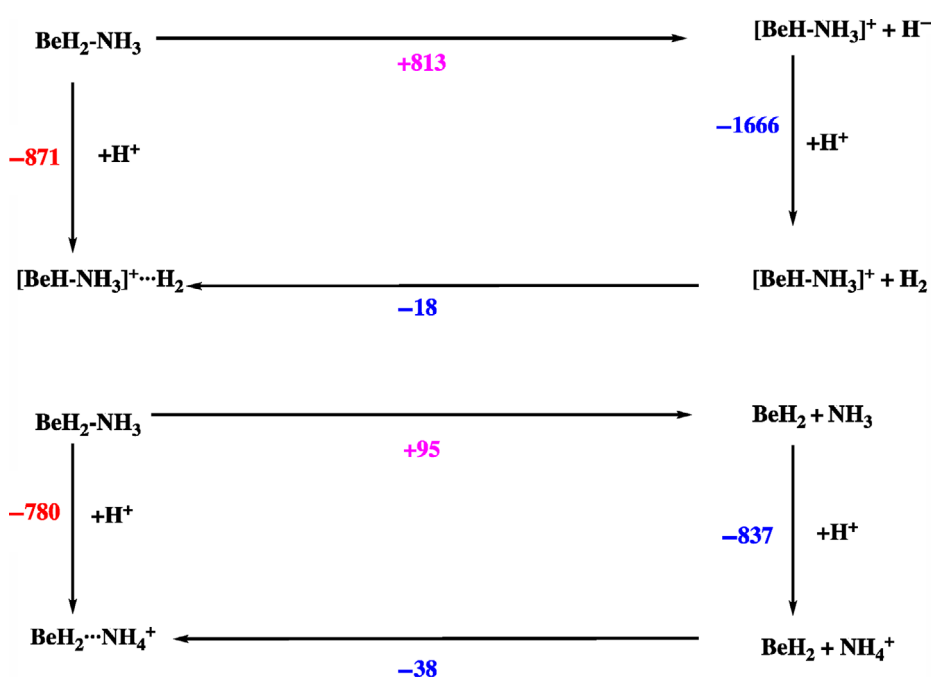[a]Only structure **A** is a minimum.

FIGURE 3 Thermodynamic cycles corresponding to the formation of $[BeH–NH_3]^+\cdots H_2$ and $[BeH_2–NH_4]^+$ protonated species of the $BeH_2–NH_3$ complex. Enthalpies are in kJ·mol^{-1}. Blue and magenta values correspond to exothermic and endothermic processes, respectively. The enthalpy of the whole process is in red.

TABLE 2 Hydride donor ability (HDA) of MH$_2$–Base complexes (M = Be, Mg, Base = NH$_3$, CH$_2$NH, HCN, NC$_5$H$_5$) and its increase (ΔHDA) relative to the isolated MH$_2$ compound. All values in kJ·mol^{-1}.

M = Be			M = Mg	
	HDA[a]	ΔHDA	HDA[a]	ΔHDA
MH$_2$	1120.9	0.0	904.0	0.0
MH$_2$–NH$_3$	813.0	−307.9	757.4	−146.6
MH$_2$–NHCH$_2$	802.6	−318.3	750.4	−153.6
MH$_2$–NCH	822.7	−298.2	748.2	−155.8
MH$_2$–NC$_5$H$_5$	765.2	−355.6	727.8	−176.2

[a]Note that, as with intrinsic acidities, the lower the HDA value, the better the system is as a H$^-$ donor.

TABLE 3 Proton affinities (PA) and proton affinity enhancements (ΔPA) of MF$_2$ and MF$_2$–Base complexes (M = Be, Mg, Base = NH$_3$, CH$_2$NH, HCN, NC$_5$H$_5$). All values are in kJ·mol^{-1}.

	M = Be			M = Mg		
Compound	A	B	ΔPA	A	B	ΔPA
MF$_2$	531.5	–	0.0	676.9	–	0.0
MF$_2$–NH$_3$	722.4	**765.3**	233.8	783.8	**818.1**	141.2
MF$_2$–NHCH$_2$	738.9	**769.5**	238.0	786.4	**814.1**	137.2
MF$_2$–NCH	**725.8**	708.4	194.3	766.5	**795.3**	118.4
MF$_2$–NC$_5$H$_5$	759.9	**806.9**	275.5	807.6	**848.3**	171.4

Note: Values in bold refer to the most basic isomer.

ionization constants. This makes BeH$_2$–NH$_3$ complex 34 kJ·mol^{-1} more basic than ammonia, indicating that a typical Lewis acid like BeH$_2$, when attached to ammonia, becomes more basic than ammonia itself. However, when examining the changes in the basicity of the N-base, the opposite trend is observed: the basicity of ammonia *decreases* by 57 kJ·mol^{-1} when it is attached to BeH$_2$. The same behavior is observed for the other bases investigated, with the decrease in basicity being more pronounced the higher the intrinsic basicity of the base. For example, when attached to BeH$_2$, methaneimine and pyridine exhibit decreases in basicity of 71 kJ·mol^{-1} (from 885 to 754 kJ·mol^{-1}) and 92 kJ·mol^{-1} (from 918 to 826 kJ·mol^{-1}), respectively (See Table 1), whereas for HCN—a much weaker N-base than the others—a slight increase of 7 kJ·mol^{-1} (from 698 to 705 kJ·mol^{-1}), rather than a decrease (see Table 1) is predicted. This peculiar behavior of HCN, stemming from its low basicity will be found again in following sections.

The increase in the basicity of the MH$_2$ moiety is directly linked to a corresponding enhancement in its hydride donor ability (HDA) (see Table 2), defined by the enthalpy of the reaction:

$$MH_2 - Base \rightarrow [MH - Base]^+ + H^- \qquad (6)$$

This reaction highlights the significant stabilization provided by the base, which enhances the overall basicity and hydride donor ability of the complex. Indeed, as illustrated in Figure S3, there is a good linear correlation between the calculated PAs and HDAs. The substantial increase in the HDA of the MH$_2$–Base complexes arises from the significant electron density transfer from the base to the MH$_2$ moiety. This transfer enhances the electron density at the H atoms, thereby increasing the HDA of the complex. This finding is further corroborated by the good correlation between the changes in HDA (ΔHDA) and PA (ΔPA) for the different bases (see Figure S4). The largest increase is observed for the pyridine complex, while the smallest one is seen for the HCN complex. In the case of pyridine, the positive charge at the [BeH–pyridine]$^+$ is easily delocalized within the aromatic ring, leading to enhanced stabilization of the closed-shell cation, a delocalization that is not

possible for the [BeH–HCN]$^+$ cation. This correlation underscores the influence of electron density transfer on the hydride donor ability and proton affinity of the MH$_2$–Base complexes.

2.2 | MF$_2$–Base complexes (M = Be, Mg)

The proton affinities of the MF$_2$–Base complexes are summarized in Table 3, and the structures of their protonated forms in Figure 4. Similar to the corresponding hydrides, protonation of MF$_2$–Base complexes can proceed either via a fluoride abstraction reaction, yielding as final product a [MF-Base]$^+$···FH complex (structures **A** in Figure 4) or via direct protonation of the base, yielding a [MF$_2$-HBase]$^+$ protonated form (structures **B** in Figure 4).

However, unlike the hydrides, protonation at the N atom of the base yielding structure **B** is energetically more favorable for the fluorides, with the only exception of the HCN complex. This different behavior between hydrides and fluorides can be explained using similar thermodynamic cycles, as shown in Figure 3.

There are two main differences compared to the hydrides. The first difference is related to the fluoride donor ability (FDA), defined by the enthalpy of the process:

$$MF_2 - Base \rightarrow [MF - Base]^+ + F^- \qquad (7)$$

as compared with the HDA of the corresponding hydride. Taken the BeF$_2$–NH$_3$ complex as an example, Figures S5 and S6 show that forming F$^-$ from BeF$_2$–NH$_3$ is more endothermic than the removing H$^-$ from BeH$_2$–NH$_3$.

The second difference concerns the formation of the HF molecule via protonation of F$^-$, which is less exothermic (−1547 kJ·mol^{-1}) than the formation of H$_2$ by protonation of H$^-$ (−1666 kJ·mol^{-1}) (Figures 3 and S5).

Importantly, for the fluoride complexes, the enhancement in basicity relative to the isolated MF$_2$ compounds remains significantly high. Nevertheless, although the basicity of the MF$_2$–Base complex is much greater than that of the isolated MF$_2$ molecule, it is generally smaller than that of the isolated base. A similar enhancement is observed in the fluoride donor ability (see Table S2).
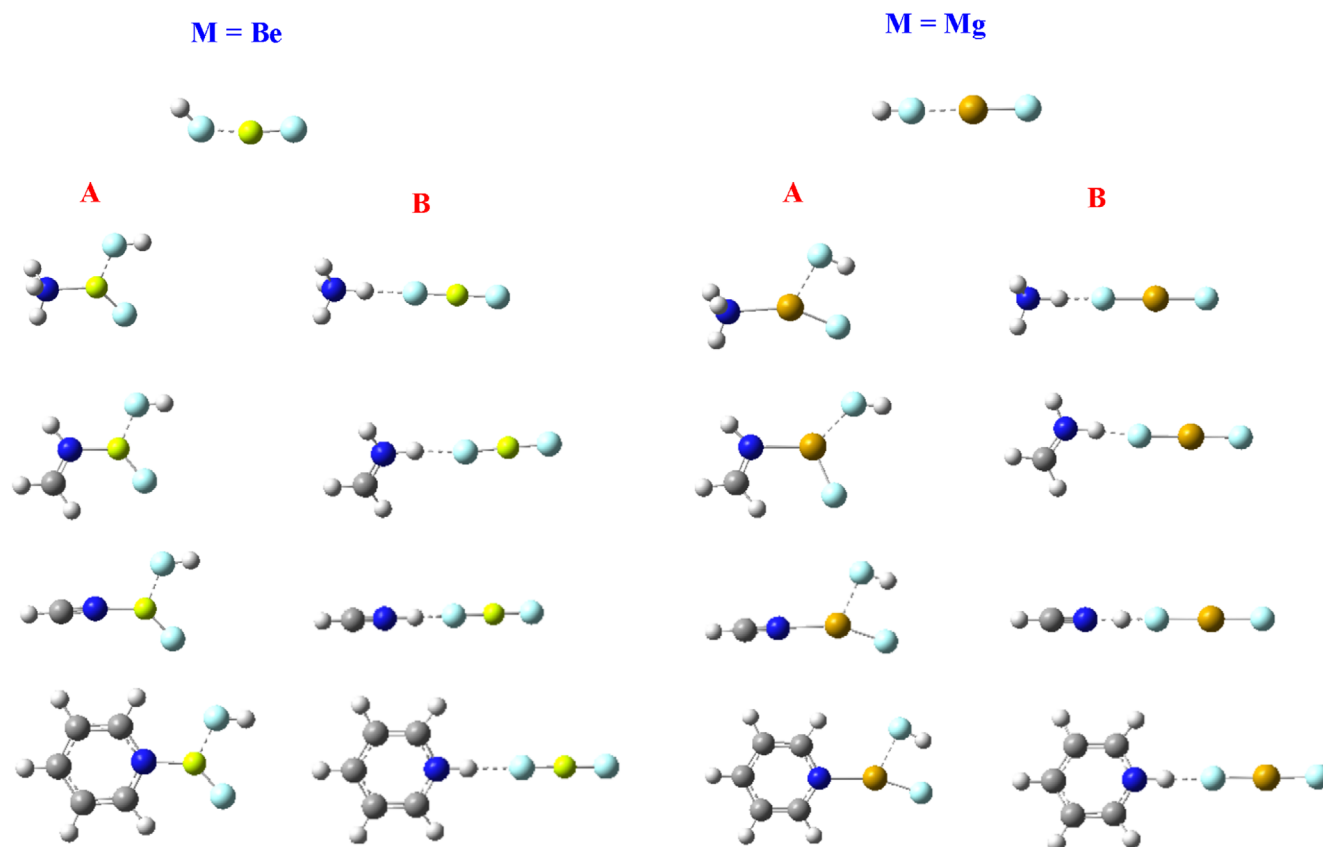
M = Be   **M = Mg**

FIGURE 4   Structures of the protonated forms of BeF_2, MgF_2, and their complexes with NH_3, CH_2NH, HCN, and NC_5H_5.

It is notable that the HCN complex exhibits unique behavior, making isomer **A** more stable than isomer **B**. This stability difference is due to the low intrinsic basicity of HCN compared to the other bases in our survey. As illustrated in Figures S5 and S6, which compares the energetics of the processes leading to isomers **A** and **B** for NH_3 and HCN, it is evident that the differences in fluoride abstraction leading to structure **A** are minimal. This similarity arises because both compounds have comparable FDAs (953 and 952 kJ·mol^{-1}, respectively; see Table S2) and similar interaction energies between the corresponding closed-shell cations and HF (−128 and −131 kJ·mol^{-1}, respectively; see Figure S5). The same applies to the various steps associated with the formation of structure **B**, with the notable exception of the PA of the base. For HCN, the PA is 139 kJ·mol^{-1} lower than for NH_3, resulting in the formation of structure **B** being 23 kJ·mol^{-1} less exothermic than the formation of structure **A**.

2.3 | M_2H_4-base complexes (M = Be, Mg)

The scenario changes significantly when moving from MH_2 monomers to M_2H_4 dimers, which have several conformations.[13] The MEP of the two more stable conformers[13] **1** and **2** (see first row of Figure 5) show again that the π-holes are on top of the Be atoms,

whereas the most attractive electrophilic areas are associated with the terminal hydrogen atoms. The hydrogen atoms participating in the (3c,2e) bonds are much less attractive. Hence, protonation is expected to occur at these terminal MH groups, leading to a typical hydride abstraction process. For the neutral conformer **1**, this process yields conformer **A** (see Figure 5). The neutral conformer **2** have two possible sites for hydride abstraction, resulting in two different conformers, **C** and **D** (Figure 5). As with the monomers, protonation at the N center of the base leads to a local minimum **B**, stabilized through a DHB between the protonated base and the M_2H_4 moiety. Finally, for ammonia and methaneimine, minima of type **E** are also possible through the formation of two DHBs.

The PAs of this set of compounds are summarized in Table 4. Systematically, the most stable protonated form results from a hydride abstraction reaction. Curiously, for Be hydrides, the most stable protonated form is **A**, whereas for Mg hydrides, it is the **C** isomer the most stable. Protonation at the N atom of the base is always much less exothermic, with the least stable forms being the **E**-type conformers.

Given that the dominant protonation processes involve hydride abstraction reactions, a direct correlation between the calculated PAs and the corresponding HDAs would be expected, as was the case for the monomers. However, this is not observed. As shown in Table 5,
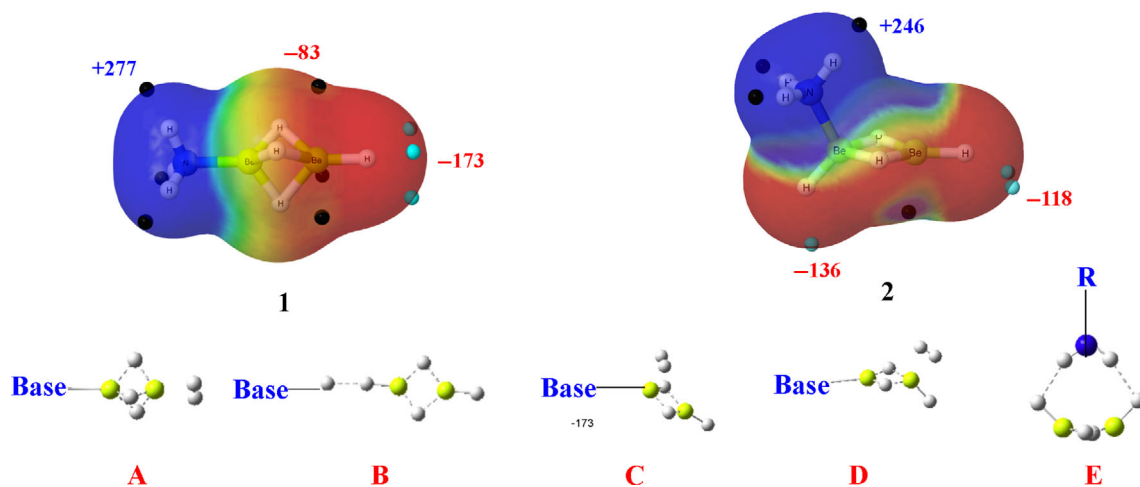
FIGURE 5 Molecular electrostatic potentials for the two most stable conformers of Be_2H_4–NH_3 and structures found to be local minima after protonation of M_2H_4–Base complexes.

TABLE 4 Proton affinities (PA) and proton affinity enhancements (ΔPA) of M_2H_4 and M_2H_4–Base complexes (M = Be, Mg, Base = NH_3, CH_2NH, HCN, NC_5H_5). All values are in $kJ \cdot mol^{-1}$.

	A	B	C	D	E	ΔPA
Be_2H_4	712.0					0.0
Base						
NH_3	**915.5**	767.6	880.8		743.4	**203.6**
$NHCH_2$	**920.3**	769.1	891.6	891.6	744.9	**208.3**
NCH	**910.0**	697.3	880.5	873.3	632.2	**98.0**
NC_5H_5	**944.8**	814.2	922.4	926.5		**232.8**
Mg_2H_4	832.5					
Base						
NH_3	887.7	834.0	**946.5**	938.8	818.7	**114.0**
$NHCH_2$	893.1	837.0	**951.2**	943.8	816.8	**118.6**
NCH	892.2	a	**949.4**	941.1	a	**116.9**
NC_5H_5	903.4	877.5	**973.9**	968.4	a	**141.4**

Note: Values in bold refer to the most basic isomer.
[a]This structure does not exist.

for both Be and Mg complexes, the highest HDA is found for conformer **C**. Accordingly, conformer **C** should be the most basic, which holds true for Mg complexes but not for Be ones.

Since the closed-shell cations in the protonated conformers **C** are more stable than in **A**, the interaction with H_2 in **A** must be stronger than in **C**. This is illustrated in Figure S7 for complexes with NH_3 and CH_2NH taken as suitable examples. For NH_3 and CH_2NH, the $[M_2H_3$–Base]$^+$ cation in **A** is 14.5 and 21.9 $kJ \cdot mol^{-1}$ less stable, respectively, than in **C**. However, the interactions of these cations with H_2 are 49.5 and 50.6 $kJ \cdot mol^{-1}$ more stabilizing for **A** than for **C**. As a result, the PAs of **A** are 34.9 (Base = NH_3) and 28.7 (Base = CH_2NH) $kJ \cdot mol^{-1}$ greater than the PAs of **C**. The question to be answered is what makes the interaction of the cation **A** with H_2 stronger than with cation **C**. A clear clue can be obtained through a MBIE analysis (see Table 6).

The first important difference is observed for the monomer distortion energies, which for the central Be atom are more than 70% larger in **A** than in **C**. This is so because, in **A**, the central Be atom changes its hybridization from sp^2 to sp^3. However, this effect is more than compensated by the possibility of forming three (3c,2e) Be–H–Be bonds in **A**. As a result, the two-center and three-center stabilization interactions in **A** are 9% and 98% greater, respectively, than in **C**. The same effects are observed for the Mg complexes, but the differences are smaller because the absolute values are also smaller. The rehybridization of Mg, being a second-row element, is less costly than for Be, resulting in a monomer distortion energy for Mg ($105 \, kJ \cdot mol^{-1}$) that is much smaller than for Be ($233 \, kJ \cdot mol^{-1}$). Thus, while for Be the one-center terms in **A** are $150 \, kJ \cdot mol^{-1}$ greater than in **C**, for Mg this difference reduces to $46 \, kJ \cdot mol^{-1}$. The same applies to the two-center and three-center stabilizing interactions, making **C** more stable than **A** for Mg complexes.

What is more important in the context of this study, the basicity enhancement observed for the MH_2–Base complexes increases when the MH_2 monomer in the complex is replaced by the M_2H_4 dimer. The basicity of the isolated dimer is significantly higher than that of the monomer, as evidenced by their HDA values (see Tables 2 and 5), with the dimer's HDA exceeding that of the monomer by $86 \, kJ \cdot mol^{-1}$. This is also consistent with the changes observed in the corresponding MEPs, which show that the electrophilic potential is greater in the dimer (-62 vs. $-48 \, kJ \cdot mol^{-1}$) (see Figure S8). Interestingly, a similar behavior was observed for their intrinsic acidities.[13]

2.4 | M_2F_4–base complexes (M = Be, Mg)

For M_2F_4–Base protonated complexes, the possible conformers are entirely similar to set **A**–**E** in Figure 5 for the hydrides. The only differences are that in conformers **A**, **C**, and **D**, the molecule interacting with the $[M_2F_3$–Base]$^+$ is HF instead of H_2 and that complexes

	A	C	ΔHDA	Base	A	C	ΔHDA
Be$_2$H$_4$	1034.1	–	0.0	**Mg$_2$H$_4$**	867.1	–	0.0
Base							
NH$_3$	827.0	**812.4**	−221.7	NH$_3$	806.6	**736.9**	−130.2
NHCH$_2$	822.0	**800.0**	−234.1	NHCH$_2$	801.0	**731.6**	−135.5
NCH	833.2	**819.8**	- 214.3	NCH	801.8	**734.5**	−132.6
NC$_5$H$_5$	795.2	**762.3**	−271.9	NC$_5$H$_5$	789.6	**706.5**	−160.5

TABLE 5 Hydride donor ability (HDA) of M$_2$H$_4$–Base complexes (M = Be, Mg, Base = NH$_3$, CH$_2$NH, HCN, NC$_5$H$_5$). All values are in kJ·mol^{-1}.

Note: Values in bold refer to the isomers with lower HDA.

TABLE 6 MBIE analysis of [M$_2$H$_3$ –Base]$^+$···H$_2$ complexes (M = Be, Mg; Base = NH$_3$, CH$_2$NH). All values are in kJ·mol^{-1}.

	$E_r(1)$	$E_r(2)$	$E_r(3)$	$\Delta E_2(12)$	$\Delta E_2(13)$	$\Delta E_2(23)$	$\Delta E_3(123)$	E_b
[Be$_2$H$_3$ –NH$_3$]$^+$···H$_2$								
A	34.4	233.0	0.4	−494.5	−40.9	−211.2	−86.5	−565.5
C	52.4	64.1	0.5	−303.0	−348.4	10.6	−1.6	−525.5
[Be$_2$H$_3$–CH$_2$NH]$^+$···H$_2$								
A	31.0	227.5	2.2	−484.9	−46.0	−222.8	−83.6	−576.5
C	51.5	61.6	2.2	−299.2	−371.6	10.7	1.7	−543.0
[Mg$_2$H$_3$ –NH$_3$]$^+$···H$_2$								
A	8.4	105	0.3	−267.8	−23.1	−118.2	−34.2	−329.7
C	22.7	46.5	0. 6	−235.0	−219.4	3.9	−7.3	−388.0
[Mg$_2$H$_3$–CH$_2$NH]$^+$···H$_2$								
A	8.25	95.4	1.1	−262.7	−27.7	−120.5	−35.0	−341.2
C	21.82	45.4	1.2	−232.8	−231.9	4.2	−8.8	−400.9

Note: The numbering of the centers is M(1)-M(2)-N(3).

B and **E** are stabilized through F···H HBs rather than dihydrogen bonds.

The trend in the PAs of Be$_2$F$_4$–Base complexes (see Table 7) is similar to that found for the corresponding BeF$_2$–Base complexes (see Table 3) for similar reasons. Thus, conformer **B** is the most basic, with the sole exception of the HCN complex. However, this trend is reversed in the Mg$_2$F$_4$–Base complexes series (see Table 7), where conformer **A** becomes the most stable. This change results from subtle differences in the energetics of the various contributing terms. The thermodynamic cycles in Figure S9 and the energetics diagrams in Figure S10 show that for the MgF$_2$–NH$_3$ complex, the formation of isomer **B** is more favorable than isomer **A** (818 vs. 784 kJ·mol^{-1}). When moving to the Mg$_2$F$_4$–NH$_3$ dimer complex, the basicity of **B** increases slightly (from 818 to 834 kJ·mol^{-1}) due to the slightly stronger interaction of the NH$_4^+$ cation with the dimer Mg$_2$F$_4$ compared to the monomer (118 vs. 100 kJ·mol^{-1}). However, the increase in the basicity of **A** from the monomer to the dimer is more significant (from 784 to 854 kJ·mol^{-1}). This is primarily due to the notable decrease in the fluoride donor ability (FDA) of the dimer compared to the monomer (801 vs. 878 kJ, mol^{-1}, see Tables S2 and S3), indicating that the dimer is a better fluoride donor. The final result is, that although the stability of both isomers **A** and **B** increases when moving from MgF$_2$ to Mg$_2$F$_4$ complexes, the increase for **A** is much larger, reversing the relative stability order.

TABLE 7 Proton affinities (PA) and proton affinity enhancements (ΔPA) for M$_2$F$_4$ and M$_2$F$_4$–Base complexes (M = Be, Mg, Base = NH$_3$, CH$_2$NH, HCN, NC$_5$H$_5$). All values are in kJ·mol^{-1}.

	A	B	C	D	E	ΔPA
Be$_2$F$_4$	507.2	–	**582.4**	–	–	0.0
Base						
NH$_3$	698.4	**778.4**	724.9	722.5	739.0	**196.1**
NHCH$_2$	702.4	**779.2**	734.3	742.4	740.7	**196.8**
NCH	694.3	718.3	**728.8**	718.5	–	**146.4**
NC$_5$H$_5$	724.8	**797.1**	762.8	765.6	–	**238.6**
Mg$_2$F$_4$	**767.7**	–	710.2	–	–	0.0
Base						
NH$_3$	**852.8**	834.7	798.1	803.2	849.2	**85.1**
NHCH$_2$	**854.5**	830.1	803.0	810.1	840.7	**86.8**
NCH	**860.7**	787.0	808.7	814.6	–	**93.0**
NC$_5$H$_5$	869.5[a]	**870.0[a]**	824.5	837.9	–	**102.3**

Note: Values in bold refer to the most basic isomer.
[a]For pyridine isomers **A** and **B** are practically degenerate.

The exceptional behavior observed for the HCN complex has the same origin as the one discussed above for the corresponding monomer.
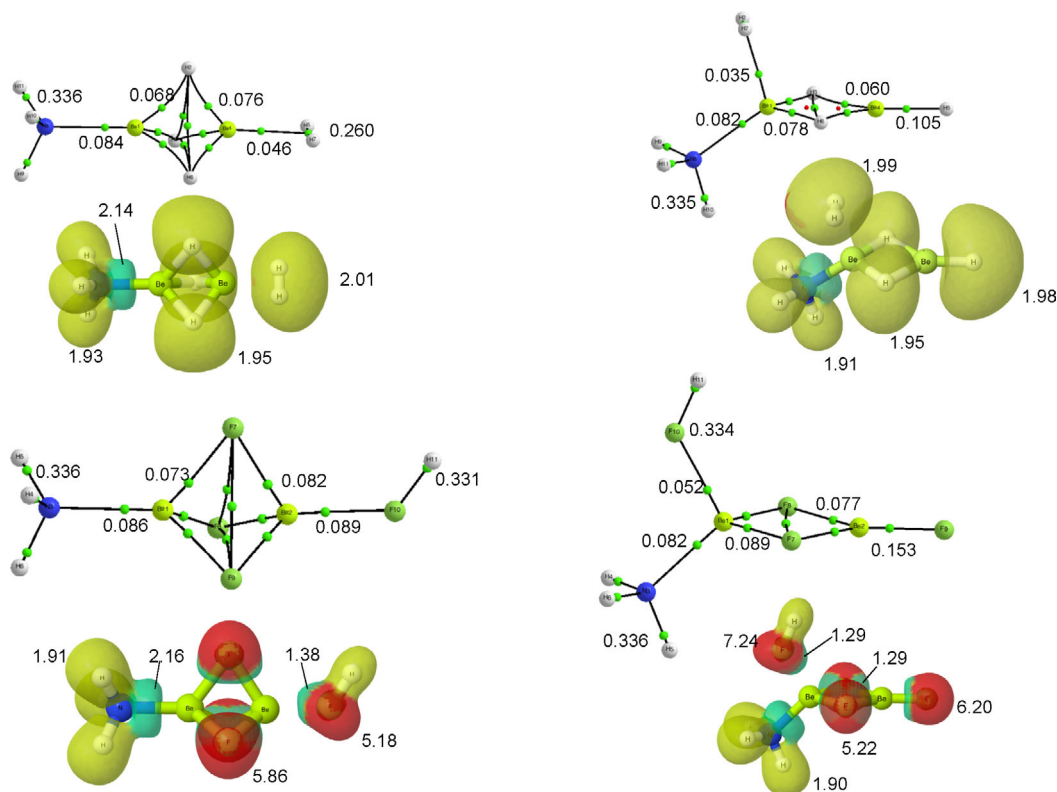
FIGURE 6 Molecular graphs and ELF plots for the conformers **A** and **C** of the Be_2X_4–NH_3 (X = H, F) complexes. In the ELF plots, all basins involving H atoms are in yellow. Monosynaptic basins are in red, disynaptic basins are in green. Their populations are in e. The electron densities at the BCPs are in a.u.

2.5 | Fluorides versus hydrides

The electron density redistributions in the complexes under study differ significantly between hydrides and fluorides, leading to distinct geometric distortions and variations in the strength of intermolecular interactions during hydride and fluoride abstraction reactions. These differences are evident when examining the molecular graphs of complexes, such as complex **A** with ammonia (see first row in Figure 6). In hydrides, three hydrogen atoms are simultaneously connected to both Be (or Mg) atoms, forming typical (3c, 2e) bonds. These bonds are characterized by low positive values for the Laplacian of the density at the corresponding bond critical points (BCPs) (see Figure S11). In contrast, while fluorides exhibit a similar connectivity pattern, the Laplacian at their BCPs is significantly more positive—approximately three times higher—indicating bonds with a much higher degree of ionicity (see Figure S11). This description aligns with the observations from the electron localization function (ELF) plots (see second row in Figure 6). In hydrides, the ELF indicates that the basins associated with the three bridging hydrogens are trisynaptic with a population of two electrons. Conversely, in fluorides, no (3c, 2e) bonds are formed, and the interaction is dominated by electrostatic contributions. The bridging F atoms exhibit a monosynaptic basin with a population close to six electrons, corresponding to its three electron pairs, and a disynaptic basin with one Be atom, populated by a single electron.

The second important difference concerns the interaction of the $[MH-Base]^+$ and $[M_2H_3-Base]^+$ cations with the H_2 molecule

TABLE 8 LMO-EDA analysis for the $[BeH-Base]^+\cdots H_2$, $[Be_2H_3-Base]^+\cdots H_2$, $[BeF-Base]^+\cdots HF$ and $[Be_2F_3-Base]^+\cdots HF$ complexes. All values are in kJ·mol^{-1}.

Hydrides: Interaction with H_2 molecule			
Component	$[BeH-NH_3]^+$ A	$[Be_2H_3-NH_3]^+$ A	$[Be_2H_3-NH_3]^+$ C
Electrostatic	−42.6	−31.9	−41.9
Exchange	−60.9	−30.9	−57.1
Repulsion	173.4	105.2	166.1
Polarization	−84.5	−95.4	−80.6
Dispersion	−34.2	−37.6	−44.1
Fluorides: Interaction with HF molecule			
Component	$[BeF-NH_3]^+$ A	$[Be_2F_3-NH_3]^+$ A	$[Be_2F_3-NH_3]^+$ C
Electrostatic	−154.7	−130.7	−131.6
Exchange	−63.1	−37.9	−57.4
Repulsion	223.5	164.0	204.1
Polarization	−118.4	−124.2	−101.8
Dispersion	−47.0	−42.9	−52.2

compared to the interaction between the $[MF-Base]^+$ and $[M_2F_3-Base]^+$ cations and HF molecule. The strength of these interactions is very similar for the different bases, the $[M_2H_3-Base]^+\cdots H_2$ interactions

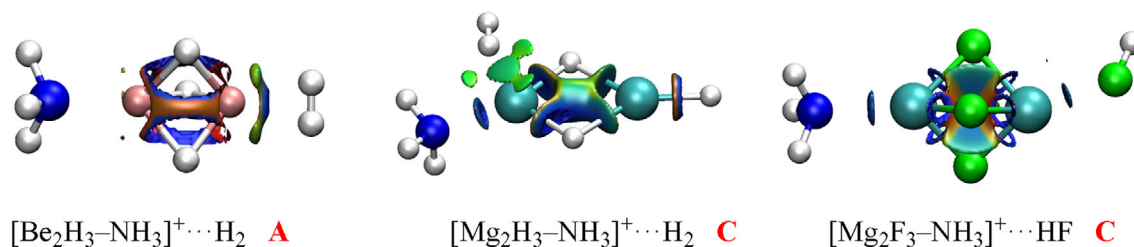$[Be_2H_3-NH_3]^+\cdots H_2$ **A** $[Mg_2H_3-NH_3]^+\cdots H_2$ **C** $[Mg_2F_3-NH_3]^+\cdots HF$ **C**

FIGURE 7 NCI plots for the most stable conformers of $[Be_2H_3-Base]^+\cdots H_2$, $[Mg_2H_3-Base]^+\cdots H_2$ and $[Mg_2F_3-Base]^+\cdots HF$ complexes. Green and blue areas correspond to weak and strong stabilizing interactions, respectively.

being around 20 kJ·mol^{-1} and $[M_2F_3-Base]^+\cdots HF$ interactions being around 130 kJ·mol^{-1}. This is consistent with the electron densities at the BCPs in Figure 6 and the results obtained through the LMO-EDA formalism (see Table 8) for the complexes with NH_3. Similar trends are observed for other complexes, as demonstrated by the examples provided in Table S4.

Regarding the stabilizing terms, for hydrides, polarization and dispersion are the dominant contributions over the electrostatic component, aside from exchange interactions. Conversely, for fluorides, the electrostatic component is more than three times larger than for hydrides, and polarization is about 1.5 times larger. These differences indicate that for fluorides, the binding of the closed-shell cation with HF is a typical ion-dipole interaction dominated by electrostatic and polarization contributions. In contrast, this is not the case for interactions with H_2, a nonpolar molecule, where polarization and dispersion are the primary stabilizing factors. This is consistent with the NCI plots for the most stable protonated forms of the Be_2H_4, Mg_2H_4, and Mg_2F_4 complexes with NH_3 (see Figure 7), which show that the non-covalent interactions (NCI) between the closed-shell cation and H_2 are weaker than those with HF but stronger for the Be-containing complexes compared to the Mg-containing ones.

Finally, we examined the stability trends of the protonated forms of $(MCl_2)_n-NH_3$ ($n = 1$, 2; M = Be, Mg) complexes to determine if they are similar to those of the corresponding fluorides. Our findings, illustrated in Figure S12, confirm that they are indeed similar.

3 | CONCLUSIONS

The gas-phase protonation of MH_2–Base and M_2H_4–Base (M = Be, Mg; Base = ammonia, methaneimine, hydrogen cyanide, pyridine) occurs at the negatively charged hydrogen atoms through typical hydride abstraction reactions. Surprisingly, in all cases, the protonation at the N atom of the base is systematically less exothermic. The preference for the hydride transfer mechanism is directly associated to the significant exothermicity of the reaction in which H_2 molecule is formed through the interaction between H$^-$ and H$^+$. The basicity of both, MH_2 or M_2H_4, increases enormously upon association of the corresponding Lewis acid with the different bases, to the point that for the hydrides basicity of the metal center is larger than the basicity of the base attached to it. In other words, typical Lewis acids become

more basic than typical nitrogen bases. In terms of the ionization constants, the increase is above 40 orders of magnitude. Conversely, the basicity of the N–Base decreases when it is attached to a MH_2 or M_2H_4 Lewis acid, the decrease being greater the higher the basicity of the N–Base.

In general, the basicity of fluorides is smaller than for hydrides, and for Be complexes, the protonation at the N atom of the base dominates. This is because, on the one hand, the loss of F$^-$ from the fluoride complexes is more endothermic than the loss of H$^-$ for the hydrides and, on the other hand, because the formation of the HF is less exothermic than the formation of H_2. Nevertheless, for the Mg complexes, the protonation process involving a fluoride abstraction mechanism is energetically the most favorable process, reflecting the greater facility of Mg complexes to lose F$^-$, due to the weaker Mg–F bonds.

DATA AVAILABILITY STATEMENT

The data that supports the findings of this study are available in the supplementary material of this article.

ORCID

Manuel Yáñez https://orcid.org/0000-0003-0854-585X

Ibon Alkorta https://orcid.org/0000-0001-6876-6211

REFERENCES

[1] M. Hurtado, M. Yáñez, R. Herrero, A. Guerrero, J. Z. Dávalos, J. L. M. Abboud, B. Khater, J. C. Guillemin, *Chem. Eur. J.* **2009**, *15*, 4622.

[2] O. Rybacka, J. Brzeski, I. Anusiewicz, P. Skurski, *Chem. Phys. Lett.* **2018**, *706*, 488.

[3] L. A. Mück, A. Y. Timoshkin, G. Frenking, *Inorg. Chem.* **2012**, *51*, 640.

[4] A. Martín-Sómer, A. Lamsabhi, O. Mó, M. Yáñez, *J. Phys. Chem. A* **2012**, *116*, 6950.

[5] A. Martín-Sómer, A. Lamsabhi, M. Yáñez, J. Z. Davalos, J. Gonzalez, R. Ramos, J. C. Guillemin, *Chem. Eur. J.* **2012**, *18*, 15699.

[6] M. Yáñez, O. Mó, I. Alkorta, J. Elguero, *Chem. Eur. J.* **2013**, *19*, 11637.

[7] O. Mó, M. Yáñez, I. Alkorta, J. Elguero, *J. Mol. Model.* **2013**, *19*, 4139.

[8] J. Kwak, N. Van Nghia, J. Lee, H. Kim, M. H. Park, M. H. Lee, *Dalton Trans.* **2015**, *44*, 4765.

[9] M. M. Montero-Campillo, O. Brea, O. Mó, I. Alkorta, J. Elguero, M. Yáñez, *Phys. Chem. Chem. Phys.* **2019**, *21*, 2222.

[10] K. Mykolayivna-Lemishko, M. Merced Montero-Campillo, O. Mó, M. Yáñez, *J. Phys. Chem. A* **2014**, *118*, 5720.

[11] O. Mó, M. Yáñez, I. Alkorta, J. Elguero, *Mol. Phys.* **2014**, *112*, 592.

[12] M. M. Montero-Campillo, M. Yáñez, A. Lamsabhi, O. Mó, *Chem. Eur. J.* **2014**, *20*, 5309.

[13] O. Mó, M. M. Montero-Campillo, M. Yáñez, I. Alkorta, J. Elguero, *J. Comput. Chem.* **2024**, *45*, 1702.

[14] NIST, in *NIST Chemistry WebBook, NIST Standard Reference Database Number 69* (Eds: P. J. Linstrom, W. G. Mallard), The NIST Research Library, Gaithersburg MD **2024**, p. 20899.

[15] J. Berkowitz, J. R. Marquart, *J. Chem. Phys.* **1962**, *37*, 1853.

[16] X. F. Wang, L. Andrews, *Inorg. Chem.* **2005**, *44*, 610.

[17] X. F. Wang, L. Andrews, *J. Phys. Chem. A* **2004**, *108*, 11511.

[18] S. Grimme, A. Hansen, J. G. Brandenburg, C. Bannwarth, *Chem. Rev.* **2016**, *116*, 5105.

[19] L. A. Curtiss, P. C. Redfern, K. Raghavachari, *J. Chem. Phys.* **2007**, *126*, 084108.

[20] O. Mó, M. M. Montero-Campillo, M. Yáñez, I. Alkorta, J. Elguero, *J. Phys. Chem. A* **2023**, *127*, 5860.

[21] O. Mó, M. M. Montero-Campillo, M. Yáñez, I. Alkorta, J. Elguero, *Molecules* **2023**, *28*, 7507.

[22] R. F. W. Bader, *Atoms in Molecules. A Quantum Theory*, Clarendon Press, Oxford **1990**.

[23] T. A. Keith, TK Gristmill Software: Overland Parks KS. **2019**. http://aim.tkgristmill.com

[24] A. Savin, R. Nesper, S. Wengert, T. F. Fassler, *Angew. Chem. Int. Edit.* **1997**, *36*, 1809.

[25] R. A. Boto, F. Peccati, R. Laplaza, C. Quan, A. Carbone, J. P. Piquemal, Y. Maday, J. Contreras-García, *J. Chem. Theory Comput.* **2020**, *16*, 4150.

[26] D. Hankins, J. W. Moskowitz, F. H. Stillinger, *J. Chem. Phys.* **1970**, *53*, 4544.

[27] S. S. Xantheas, *J. Chem. Phys.* **1994**, *100*, 7523.

[28] P. F. Su, Z. Jiang, Z. C. Chen, W. Wu, *J. Phys. Chem. A* **2014**, *118*, 2531.

[29] M. W. Schmidt, K. K. Baldridge, J. A. Boatz, S. T. Elbert, M. S. Gordon, J. H. Jensen, S. Koseki, N. Matsunaga, K. A. Nguyen, S. J. Su, T. L. Windus, M. Dupuis, J. A. Montgomery, *J. Comput. Chem.* **1993**, *14*, 1347.

[30] L. Luan, J. S. Song, R. M. Bullock, *J. Org. Chem.* **1995**, *60*, 7170.

[31] D. E. Berning, B. C. Noll, D. L. DuBois, *J. Am. Chem. Soc.* **1999**, *121*, 11432.

[32] C. J. Curtis, A. Miedaner, W. W. Ellis, D. L. DuBois, *J. Am. Chem. Soc.* **2002**, *124*, 1918.

[33] D. L. DuBois, D. M. Blake, A. Miedaner, C. J. Curtis, M. R. DuBois, J. A. Franz, J. C. Linehan, *Organometallics* **2006**, *25*, 4414.

[34] J. L. Miller, J. Lawrence, F. O. R. del Rey, P. E. Floreancig, *Chem. Soc. Rev.* **2022**, *51*, 5660.

[35] J. L. Miller, K. Damodaran, P. E. Floreancig, *Chem. Eur. J.* **2023**, *29*, e202302977.

[36] A. P. Lathem, Z. M. Heiden, *Dalton Trans.* **2017**, *46*, 5976.

[37] S. Basak, L. Winfrey, B. A. Kustiana, R. L. Melen, L. C. Morrill, A. P. Pulis, *Chem. Soc. Rev.* **2021**, *50*, 3720.

[38] L. Liu, *Acc. Chem. Res.* **2022**, *25*, 3537.

[39] T. Tandaric, A. Prah, J. Stare, J. Mavri, R. Vianello, *Int. J. Mol. Sci.* **2020**, *21*, 17.

[40] M. Horn, L. H. Schappele, G. Lang-Wittkowski, H. Mayr, A. R. Ofial, *Chem. Eur. J.* **2013**, *19*, 249.

[41] Z. M. Heiden, A. P. Lathem, *Organometallics* **2015**, *34*, 1818.

[42] R. J. Mayer, J. Moran, *Org. Biomol. Chem.* **2022**, *21*, 85.

[43] R. H. Crabtree, P. E. M. Siegbahn, O. Eisenstein, A. L. Rheingold, *Acc. Chem. Res.* **1996**, *29*, 348.

[44] I. Alkorta, J. Elguero, C. Foces-Foces$, *Chem. Commun.* **1996**, *14*, 1633.

[45] V. I. Bakhmutov, *Dihydrogen Bond: Principles, Experiments, and Applications*, Wiley-Interscience, New York **2013**.

SUPPORTING INFORMATION

Additional supporting information can be found online in the Supporting Information section at the end of this article.